04

Spectral diagnostics of plasma in a cesium lamp with a pulse-periodic discharge

© A.A. Bogdanov, I.I. Stolyarov

Ioffe Institute, St. Petersburg, Russia
e-mail: a.bogdanov@mail.ioffe.ru

Received April 22, 2025
Revised May 30, 2025
Accepted June 6, 2025

A detailed study of the emission spectra of a cesium lamp with a pulse-periodic discharge at relatively low pressures made it possible to determine the electron concentration both from the recombination continuum and from the broadening of the spectral lines of cesium and xenon. The concentration values obtained by the two methods are consistent. The electron temperature was determined from the spectrum of the recombination continuum, which was recorded in the visible and short-wave range (up to 290 nm), which made it possible to determine the photorecombination cross-section here. A feature of the shift of the CsI lines of the diffuse *6p–nd* series ($n = 7-10$) was discovered. Recording the evolution of the shape of many spectral lines made it possible to draw conclusions about the behavior of the gas in a pulse and decay within the framework of a simple model.

Keywords: emission spectrum, electron concentration and temperature, recombination continuum, broadening and shift of spectral lines.

DOI: 10.61011/TP.2026.01.62843.78-25

Introduction

High-current cesium lamps with a pulse-periodic discharge have a high color rendering index (97–98) and a significant luminous efficiency (up to 70 lm/W), which makes them promising for application as high-quality light sources and production of high luminous fluxes. To identify the optimal operating modes of such lamps, they were put through testing, which included the recording of both integral luminous fluxes within a wide range of operating parameters with the determination of luminous efficiency and emission spectra with a time resolution of 1 μs [1–4].

The main design elements of a cesium lamp are a cylindrical sapphire burner, where a discharge takes place, and a vacuum-sealed cylindrical quartz bulb. Two modifications are feasible: double-ended lamps, where sealed current leads are positioned at opposite ends of a quartz bulb, and single-ended lamps, where both current leads are sealed at one end of the bulb. The latter modification is simpler, but the cross section of current leads of a single-ended lamp is significantly smaller. This translates into an increased thermal load on the current leads and may cause overheating of the current lead–quartz bulb seal and loss of vacuum. Therefore, the maximum average power (and, consequently, cesium pressure) levels achieved in single-ended lamps were lower than those corresponding to double-ended ones. The present study differs from the earlier ones [1–4] in that the discharge in a single-ended lamp is investigated in regimes with lower power (cesium pressures) levels. The aim of this is to perform diagnostics of plasma parameters in pulsed operation of a cesium lamp at relatively low cesium pressures by recording optical spectra with a sufficiently high time resolution.

1. Experimental procedure

The single-ended cesium lamp was basically a cylindrical sapphire burner placed in a cylindrical quartz bulb. The internal burner diameter was $2r = 5$ mm, and the interelectrode distance was 22 mm. Prior to sealing, Cs was introduced into the burner, and xenon (Xe) was fed at a pressure of 20 Torr (Xe atom concentration $n_{\mathrm{Xe}} = 6.7 \cdot 10^{17}\,\mathrm{cm}^{-3}$). Xenon was needed to ignite the cold lamp. The radiation spectrum was recorded using an MDR-23 monochromator; the image of the lamp was focused by a quartz lens (with a focal distance of 112 mm) onto the entrance slit of the monochromator. A FEU-79 photomultiplier served as the radiation detector. Just as the lamp itself, the cylindrical burner was positioned horizontally and perpendicular to the optical axis of the recording system; thus, all radiation from the region extending along the burner diameter entered the monochromator. The transverse size of this region was set by the entrance slit of the monochromator.

In the course of operation, pulses of linearly increasing current of variable polarity were supplied to the electrodes from a special generator. The amplitude of these pulses varied up to 150 A, their duration was 15–50 μs, and the repetition rate was 12–1500 Hz. The gated integration method provided an opportunity to record spectra at different moments within a current pulse and after it in decaying plasma with a time resolution of 1 μs. The system for data acquisition and processing also allowed us to record the time dependences of the lamp current and voltage and the lamp emission at a given wavelength.

When the discharge spectrum was recorded, the widths of input and output slits of the monochromator remained within the range of 0.1–0.01 mm, while the width of the

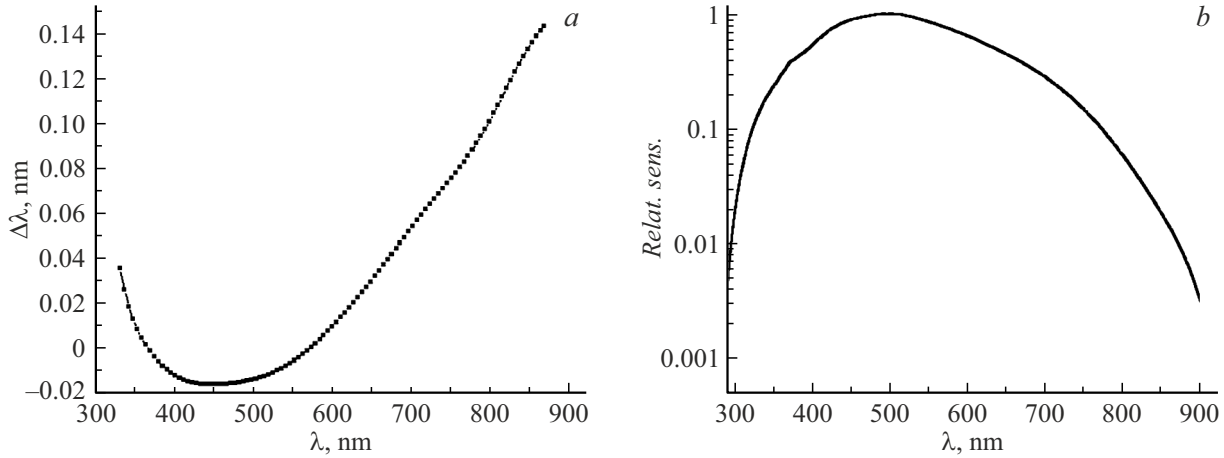

Figure 1. *a* — Calibration curve of the monochromator; *b* — relative sensitivity of the recording system.

transverse slit was 0.8 mm. Wide and narrow slits were used to record the relatively weak continuum spectrum and strong lines, respectively. All spectra were recorded by a monochromator with a 1200 groove/mm grating; its reciprocal dispersion with this grating was 1.3 nm/mm. Hence, the spectral resolution at the given slit widths was 0.13–0.013 nm. The minimum interval of spectra recording was set at 1/300 nm by the stepper motor of the monochromator. This step was used to record the narrowest lines. A step of 0.05–0.1 nm was used for the slowly varying continuum. Optical diagnostics of plasma parameters requires thorough calibration of the monochromator and determination of the spectral sensitivity of the recording system.

The monochromator was calibrated within the spectral range of 320–890 nm against the spectrum of a neon indicator lamp with a DC supply (16 mA, 300 V). At such currents, the concentration of electrons in the discharge had no effect on the position of spectral lines. A total of 120 lines of NeI, KrI, and even KrII were recorded within the specified range. The KrII lines virtually vanished when the current was reduced to 6 mA. The optical resolution of the recording system was governed by the width of the monochromator slits and was close to 0.15 nm. The positions of lines were determined with an accuracy no worse than 0.005 nm. The resulting monochromator calibration curve (Fig. 1, *a*) was obtained by smoothing the original experimental curve. All experimental points deviate from the resulting calibration curve by no more than 0.01 nm. Thus, the accuracy of determination of wavelengths in spectra recorded with this monochromator is no worse than 0.01 nm if the calibration curve is taken into account.

The spectral sensitivity of the optical signal recording system was determined using a TRSh 2850-3000 ribbon lamp. At a lamp current of 7.00 A, calibration for $\lambda = 656.3$ nm yielded a brightness temperature of 2432 K; with the transmittance of the sapphire window of the lamp and the emissivity of tungsten taken into account, the true temperature of the lamp is 2756 K. The ribbon lamp emission decays rapidly as wavelength λ decreases; at $\lambda < 320$ nm, the sensitivity of the entire recording system, which is governed by the photomultiplier tube in this region, also undergoes a sharp drop. Therefore, the ribbon lamp signal decays rapidly within this range with decreasing λ, reaching a fairly high constant level, which is set by scattered light in the monochromator, at $\lambda < 290$. This conclusion was verified by installing a UFS-1 filter at the input, which reduced greatly the integral radiation flux entering the monochromator. Consequently, the level of scattered light in the monochromator and the signal level reported by the recording system on the plateau at $\lambda < 290$ nm decreased. To determine the true signal of the ribbon lamp, one needs to subtract the scattered light magnitude from the recorded signal. Owing to the noise of scattered light and an element of uncertainty in its extrapolation, the signal of the ribbon lamp could be determined with an acceptable error only at $\lambda > 295$ nm. Thus, the sensitivity of the recording system was determined within the range of 295–900 nm (Fig. 1, *b*).

2. Measurement results

As was demonstrated in [4], the lamp starts to heat up after ignition and gradually (within a few minutes) reaches a steady thermal regime. The overall amount of Cs vapor in the burner remains unchanged in the steady thermal regime, although the radial distribution of Cs varies significantly over a period, following the change in plasma temperature. The temperature of electrons on the burner axis increases to $(5–10) \cdot 10^3$ K during a current pulse. In a narrow near-wall layer, it remains close to the temperature of the inner wall of the burner, which does not exceed 1500–2000 K. This leads to a reduction in concentration of the heavy component (atoms and ions) in the axial region and a sharp increase in this concentration in the narrow near-wall layer. The temperature distribution along the burner radius

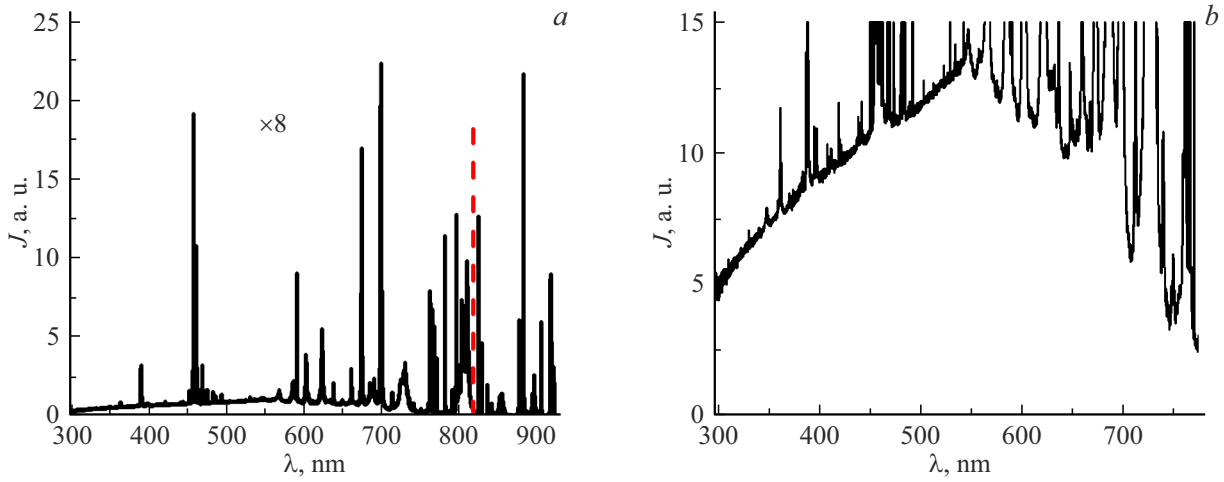

Figure 2. *a* — Discharge spectrum; *b* — recombination continuum for regime 1.

is fairly flat (especially at the end of a pulse when plasma is close to complete ionization). The electron concentration in the near-wall layer, where the temperature decreases, drops sharply toward the wall, suppressing the emission of recombination continuum from this layer. Therefore, we assume as a first approximation that the plasma parameters and significant features of the spectrum (e.g., the width of lines and their shift) do not depend on the radius. This will be taken into account in processing of the spectra. The validity of this fairly rough approximation will be confirmed by a satisfactory agreement between the values of plasma parameters obtained in different ways. It should be noted here that the error in reconstructing the radial distribution of the plasma column luminosity for a lamp of the examined design is very large. This is attributable to the fact that the single-crystal sapphire burner has a small internal diameter (5 mm) and thick walls (1 mm), and the surfaces of these walls undergo no treatment after growth.

As was noted in the Introduction, the presents study is focused on operating regimes with a reduced power of 34 and 42 W and correspondingly low cesium vapor pressure levels (regime 1: current amplitude, 50 A; pulse duration, $\tau = 50\,\mu$s; pulse repetition rate, 854 Hz; power, 34 W; regime 2: 42 A, 42 μs, 1397 Hz, and 42 W). Figure 2, *a* shows the panoramic spectrum of a discharge (with the sensitivity of the recording system illustrated in Fig. 1, *b* taken into account) in regime 1. The spectrum was recorded at the end of a current pulse. The signal within the 295–816 nm range is magnified in the figure by a factor of 8.

It can be seen that the spectrum consists mostly of strong lines and a rather weak continuous recombination continuum at $\lambda < 750$ nm (enlarged in Fig. 2, *b*). Since the concentration of cesium in the studied regimes is low, there are no traces of molecular absorption bands (including diffuse absorption bands within the 700–720 nm range, which provide an opportunity to determine the concentration of Cs atoms) of the cesium dimer molecule in the continuum [4]. The most intense emission lines are located within the infrared range. It follows from a thorough analysis of the spectrum that strong lines belong mostly to CsI and XeI. Among the strong cesium lines, one may note weak lines of forbidden doublets $6s$–$5d$ (684.88 and 689.49 nm) and $6s$–$6d$ (441.13 and 442.57 nm). The emission spectrum of the lamp features impurity lines: NaI (first and second resonance doublets), KI (first resonance doublet), and RbI (first, second, and third resonance doublets), as well as several weak lines that may be attributed to XeII and CsII.

As is known [5,6], emission intensity $I_j(\lambda)$ for recombination into state j for the Maxwellian electron distribution function is

$$J_j(\lambda)d\lambda = \left(\frac{2m}{\pi}\right)^{1/2} \frac{h^2c^2}{(kT_e)^{3/2}} \frac{n_e^2}{\lambda^3} v^2\sigma_j(v) \times \exp\left[-\frac{hc}{kT_e}(1/\lambda - 1/\lambda_j)\right] d\lambda, \qquad (1)$$

where T_e is the temperature of plasma electrons, n_e is the electron concentration, c is the speed of light, k is the Boltzmann constant, h is the Planck constant, hc/λ_j is the binding energy of state j, λ_j is the long-wavelength boundary of j-continuum, $mv^2/2$ is the initial kinetic energy of a captured electron, and $\sigma_j(v)$ is the cross section of photorecombination of an electron with velocity v into state j. In cesium, continuum emission is largely determined by the sum of $6P$- and $5D$-continua ($\lambda_{6P} = 508.4$ nm, $\lambda_{5D} = 594.6$ nm).

The cross sections of photorecombination onto the $6P$ and $5D$ levels of a cesium atom were measured in [5,6]: $\sigma_j(v)v^2 = C_j$. $C_{6P} = 3.74 \cdot 10^{-6}$ cm^4/s^2, $C_{5D} = 8.3 \cdot 10^{-6}$ cm^4/s^2. The absolute intensity at the head of $6P$-continuum specifies electron concentration n_e. It can be seen from (1) that the dependence of $\ln[J(\lambda)\lambda^3]$ on $1/\lambda$ is straight; its slope specifies hc/kT and, consequently, the electron temperature. The time of energy transfer from electrons to Cs^+ cesium ions at the start of a current pulse, when electron concentration $n_e = 10^{15}$ cm^{-3}, is $1-2\,\mu$s. The time of energy transfer from Cs^+ ions to Xe atoms at the start of a current pulse is also close to 1 μs. With

an increase in plasma concentration to $10^{16}\,\mathrm{cm}^{-3}$, these times decrease by an order of magnitude. Therefore, with a characteristic time of temperature variation in the discharge of $10\,\mu$s, the temperatures of electrons, ions, and atoms are virtually equal almost everywhere in the burner; i.e., all particles have a common plasma temperature T. Electron temperature decoupling is observed only in a very narrow near-wall region.

Figure 3 shows the discharge spectrum in coordinates $[x = 10^3/\lambda,\ y = \ln(J\lambda^3)]$ (with the sensitivity of the recording system taken into account). The long-wave boundaries of the corresponding continua are indicated with arrows. Several variants of the scattered light level were chosen (level variations remained within the noise limit of 2% at the most) for determination of the sensitivity. These variants correspond to different recalculated discharge spectra (shown in different colors). Within the range of $1000/\lambda > 3.40\,\mathrm{nm}^{-1}$ ($\lambda < 294\,\mathrm{nm}$), the indicated small changes in the level of scattered light induce a very significant alteration of the spectrum. At $\lambda > 294\,\mathrm{nm}$, the true Cs lamp signal does not depend on the specified background variations: all plots match. Notably, points fit perfectly on a straight line, verifying the applicability of the simplest model of this discharge mentioned above. Wavelength $\lambda = 294\,\mathrm{nm}$ corresponds to a quantum energy of 4.22 eV. Taking the ionization energy of a Cs atom in the $6P$ state (2.51 eV) into account, we find that the energy of the recombining electron is 1.71 eV. Thus, the $\sigma_j(v)v^2 = \mathrm{const}$ ratio, which was verified experimentally in [5] through to 0.66 eV, remains valid at least up to an electron energy of 1.71 eV. The plot in Fig. 3 yields temperature $T = 8100\,\mathrm{K}$. The continuum spectra were recorded at another 2–3 points within the pulse and decay time; all of them had the shape of straight lines in the indicated coordinates. Dependence $T(t)$ of the plasma temperature on time may be obtained by processing such continuum spectra recorded at different points within the pulse and decay time. This time-consuming procedure

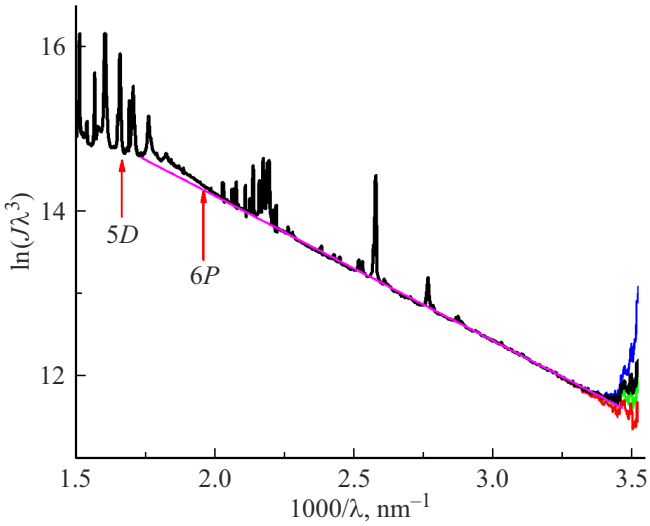

Figure 3. Discharge spectrum in regime 1 recorded at the end of a pulse ($50\,\mu$s).

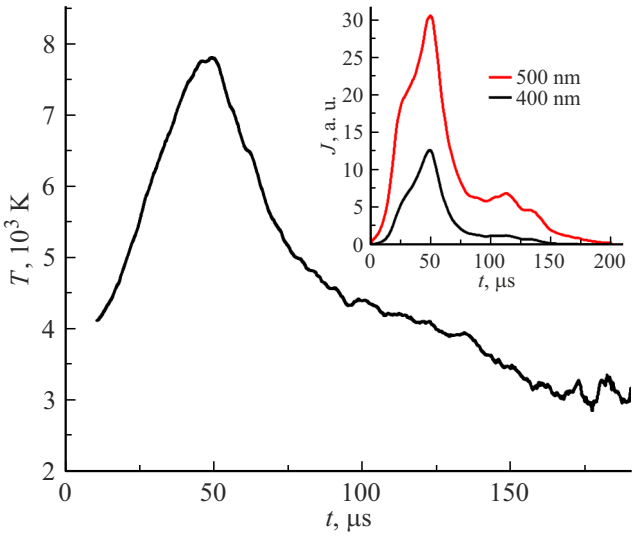

Figure 4. Temporal dependence of temperature in regime 1. Temporal dependences of the continuum at $\lambda = 500$ and 400 nm are shown in the inset.

may be shortened by recording the time dependence of continuum emission $J_\lambda(t)$ at two wavelengths λ_1 and λ_2 from the $\lambda < \lambda_{6P} = 508.4\,\mathrm{nm}$ range [7]. Naturally, λ_1 and λ_2 should be free of atomic lines. In the present study, $\lambda_1 = 500\,\mathrm{nm}$ and $\lambda_2 = 400\,\mathrm{nm}$ were chosen. The temperature was calculated as

$$T(t) = \frac{\frac{hc}{k\lambda_2} - \frac{hc}{k\lambda_1}}{\ln\left[\frac{J_1(t)s_2}{J_2(t)s_1}\left(\frac{\lambda_1}{\lambda_2}\right)^3\right]} = \frac{1.439\cdot 10^4\left(\frac{1}{400} - \frac{1}{500}\right)}{\ln\left[\frac{J_1(t)s_2}{J_2(t)s_1}\left(\frac{500}{400}\right)^3\right]}$$

$$= \frac{7.19}{\ln\left(1.044\,\frac{J_1(t)}{J_2(t)}\right)}. \qquad (2)$$

Here, s_1 and s_2 are the relative sensitivities of the recording system at the wavelengths of 500 and 400 nm.

Figure 4 shows the $T(t)$ dependence constructed this way ($t = 0$ and $50\,\mu$s correspond to the start and end of a current pulse). The original temporal dependences of the continuum at $\lambda = 500$ and 400 nm are shown in the inset. It is evident that the continuum signals become much (two orders of magnitude) weaker toward 150–200 μs; the signal at 400 nm is reduced to a virtually constant noise level. This is associated with an increased scatter in the calculation of temperature at $t > 150\,\mu$s and the impossibility of determination of temperature in long-term decay at $t > 200\,\mu$s. At the start of a pulse, the continuum signals are also weak (especially at $\lambda = 400\,\mathrm{nm}$), so T is indeterminable here as well.

Figure 5 shows the temporal dependences of plasma concentration and temperature in regime 2 calculated based on the measured continuum. It can be seen that the characteristic growth time of n_e and T in a pulse is 10–20 μs; at the start of the relaxation stage, the characteristic decay time is also 10–20 μs, but it grows to 100 μs and beyond later

on. In order to interpret the obtained results, we estimate the characteristic times of the main processes in decay and pulse intervals.

When the concentration of Xe in the burner is $n_{\mathrm{Xe}} = 6.7 \cdot 10^{17}\,\mathrm{cm}^{-3}$, the specific internal energy of Xe at the end of a current pulse ($T = 6300\,\mathrm{K}$) is $(3/2)kTn_{\mathrm{Xe}} = 0.086\,\mathrm{J/cm}^{-3}$. The specific internal energy of Cs^+ ions at the end of a pulse is $0.015\,\mathrm{J/cm}^{-3}$ at $n_e = 2 \cdot 10^{16}\,\mathrm{cm}^{-3}$ (cesium is assumed to be completely ionized). It follows from these estimates that the major part of internal energy of the gaseous medium of the lamp at the end of a pulse is stored in heated xenon. Its cooling will shape the dynamics of decay. The characteristic cooling time of xenon in the interval between current pulses in the cylindrical burner due to transfer of heat to the wall is $\tau_{T1} = r^2/(a_{\mathrm{Xe}}(\mu_1)^2)$. Here, r is the internal radius of the burner, a_{Xe} is the thermal diffusivity coefficient of xenon, and μ_1 is the constant for the fundamental mode, which is determined from the boundary conditions and depends on heat transfer at the gas–sapphire wall boundary; $a_{\mathrm{Xe}} = \lambda_{\mathrm{Xe}}/(c_V\rho)$, where λ_{Xe} is the thermal conductivity of Xe, c_V is the specific isochoric heat capacity, and ρ is the density of Xe; $\lambda_{\mathrm{Xe}} = 0.02\,\mathrm{W/(m{\cdot}K)}$ (at $T = 1300\,\mathrm{K}$) [8]. In decay, $T = (3{-}4) \cdot 10^3\,\mathrm{K}$ (Fig. 6), and the thermal conductivity increases by a factor of more than $(T)^{0.5}$ (a_{Xe} within the range of $25{-}40\,\mathrm{cm}^2/\mathrm{s}$). With large heat transfer, $\mu_1 = 2.4$. Thus, $\tau_{T1} = 300{-}400\,\mu\mathrm{s}$ under the assumption that λ_{Xe} remains constant along the radius.

Let us estimate the characteristic time of plasma diffusion decay (diffusion escape of Cs^+ to the burner wall) after the end of a current pulse: $\tau_{\mathrm{dif}} = r^2/(2D_{\mathrm{Cs}^+}(2.4)^2)$. Here, $2D_{\mathrm{Cs}^+}$ is the coefficient of ambipolar diffusion (in the $T_e = T_i$ case). The coefficient of diffusion of Cs^+ ions in Xe is $D_{\mathrm{Cs}^+} = 0.057\,\mathrm{cm}^2/\mathrm{s}$ at a pressure of 1 atm and $T = 320\,\mathrm{K}$ [9,10]. The recalculation of D_{Cs^+} for a pressure of 20 Torr and $T = 3200\,\mathrm{K}$ [9] yields $D_{\mathrm{Cs}^+} = 14.4\,\mathrm{cm}^2/\mathrm{s}$ and $\tau_{\mathrm{dif}} = 380\,\mu\mathrm{s}$. If additional scattering off Cs atoms is introduced, this time increases to $\tau_{\mathrm{dif}} = 1000\,\mu\mathrm{s}$.

At $T = 5000\,\mathrm{K}$, the cross section of stepwise ionization of Cs by electrons with a Maxwellian distribution function is $\sigma_i = 10^{-16}\,\mathrm{cm}^2$ [11,12]. At a cesium atom concentration of $2 \cdot 10^{16}\,\mathrm{cm}^{-3}$, the characteristic time of stepwise ionization is $\tau_i = (\sigma_i v_e n_{\mathrm{Cs}})^{-1} = 10^{-2}\,\mu\mathrm{s}$; at 3000 K, this time is longer by a factor of approximately 30, but is still below $1\,\mu\mathrm{s}$. The characteristic time of bulk three-particle recombination is $\tau_r = T^{(9/2)}/(5.4 \cdot 10^{-27} \cdot n_e^2)$ [13], where T, [eV]. The recombination time within the ranges of $T < 6 \cdot 10^3\,\mathrm{K}$ and $n_e > 2 \cdot 10^{15}\,\mathrm{cm}^{-3}$ is $\tau_r < 1\,\mu\mathrm{s}$. Thus, τ_i and τ_r are much shorter than the characteristic times of temperature rise and fall in the pulse and decay intervals, and the processes of ionization and recombination are almost balanced. The electron concentration follows a slow increase in temperature within a pulse and a slow T reduction in decay, reaching an equilibrium value at each point in time. This is confirmed by a comparison of the experimental $n_e(t)$ curve with the calculated dependence of equilibrium concentration on time for experimental $T(t)$ (Fig. 5). The calculation of

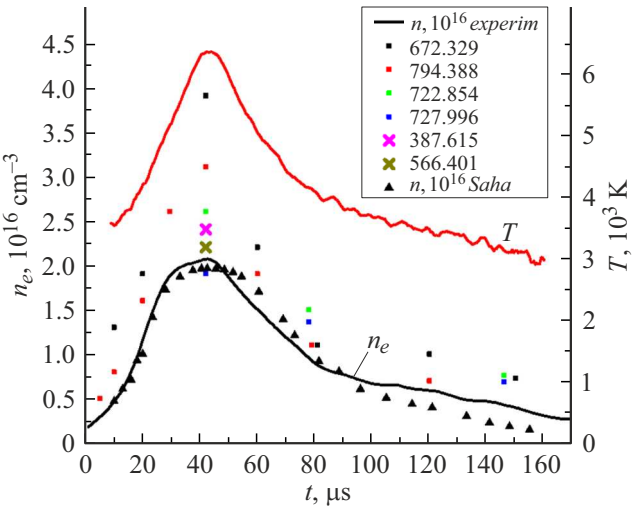

Figure 5. Temporal dependences of plasma concentration n and temperature T in regime 2.

equilibrium concentration of Xe^+ ions at $T = 6200\,\mathrm{K}$ and $n_{\mathrm{Xe}} = 6.7 \cdot 10^{17}\,\mathrm{cm}^{-3}$ yields $n_{\mathrm{Xe}} = 1.1 \cdot 10^{15}\,\mathrm{cm}^{-3}$, which is much lower than the concentration of Cs ions. The actual concentration of Xe^+ ions will be lower than the equilibrium value, since the electron distribution function at energies near the first resonance level of Xe will deviate from the Maxwellian function (electron Maxwellization frequency ν_{ee} at an energy of $8{-}10\,\mathrm{eV}$ is comparable to the frequency of inelastic collisions of electrons with Xe atoms).

Colored symbols in Fig. 5 denote the plasma concentration values at different points in time that were calculated from the half-width of the corresponding CsI spectral lines recorded at these points in time. The slit width was $0.02{-}0.03\,\mathrm{mm}$ in the process of line recording, which corresponds to spectral width of $0.02{-}0.04\,\mathrm{nm}$ for a reciprocal dispersion of 1.3 nm/mm. The actual spectral resolution of the recording system was determined by analyzing the narrow resonance lines of NaI and KI impurities and was twice the width of slits. The experimental half-width of all lines indicated in Fig. 5 is much greater than the spectral resolution in the studied regimes. Therefore, it was sufficient to subtract the spectral resolution from the half-width of the experimental profile to determine the actual half-width of a line. Theoretical and experimental values of broadening w and shift d constants for Cs, Xe, Na, K, and Rb [14,15] were used to determine n_e based on the actual line half-width. It can be seen from the figure that the n_e values determined independently based on the continuum and the line half-width are in reasonable agreement. Note that the n_e values calculated from the half-width of Xe lines are also consistent with those shown in Fig. 5. Examples of characteristic lines recorded at different points in time are presented in Figs. 6, 7.

It is evident from Fig. 6 that the CsI line (794.388 nm $6p$–$8s$) expands during a pulse and shifts toward longer waves, almost merging with the RbI line (794.760 nm $5s$–$5p$, long-wave component of the resonance doublet).

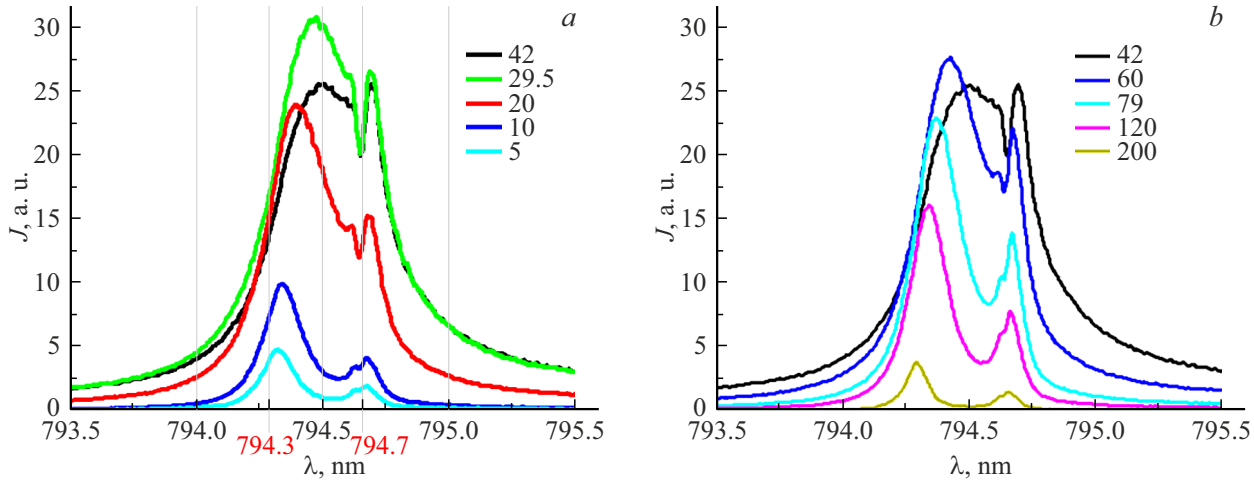

Figure 6. Section of the spectrum with lines CsI (794.388 nm $6p$–$8s$) and RbI (794.760 nm $5s$–$5p$) in regime 2 recorded at different points within the pulse (left) and decay (right) time. Numbers indicate the time in μs elapsed from the start of a pulse (the pulse length is 42 μs).

The reverse process is observed in decaying plasma: the 794.388 nm line grows narrower and shifts to the short-wavelength side. Figure 7 provides an illustration of a similar behavior of CsI lines (722.854 and 727.99 nm $5d$–$6f$) in decay.

A narrow dip in the RbI line is clearly visible in Fig. 6. This dip is attributable to self-absorption of RbI emission in the cold near-wall layer with an increased concentration of the heavy component. Its position does not change during a pulse and in decay, and its wavelength matches closely the tabular value (indicated by the mark with a red number in the figure). The relative depth of the dip may be used to assess the growth of the near-wall layer. Within 5 μs of the start of a pulse, the layer is virtually nonexistent; by 30 μs, it is essentially formed. In decay, only a step is left of the dip by 79 μs (T has dropped to 3500 K by this time). Similar dips associated with self-absorption in the near-wall layer were also observed in certain CsI lines (first and second resonance doublets and the $6p$–$6d$ and $6p$–$7d$ lines). This is hardly surprising, since absorption in these lines is attributable to transitions from the ground and first excited states of a Cs atom. Thus, examination of the shape variation of lines over time provided an opportunity to identify qualitatively the processes of plasma generation and decay (by the broadening and shift of lines) and to establish the fact of displacement of atoms to the wall of the burner (by the emergence and growth of the dip).

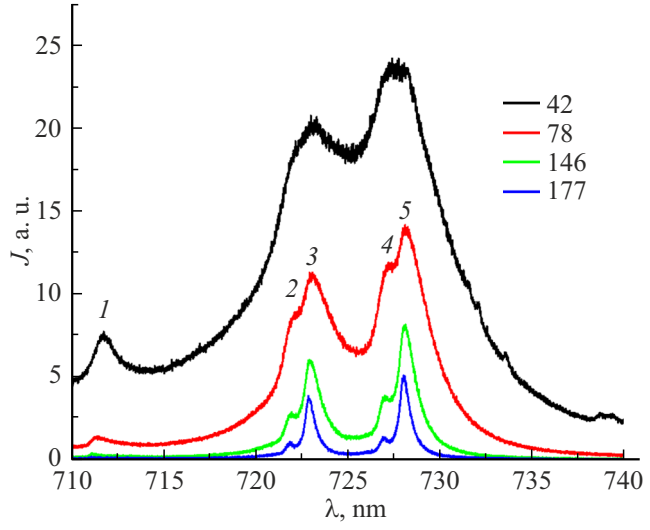

Figure 7. Lines: *1* — XeI 711.960, *2* — CsI 721.970 $5d$–$6g$, *3* — CsI 722.854 $5d$–$6f$, *4* — CsI 727.070 $5d$–$6g$, and *5* — CsI 727.990, 727.996 $5d$–$6f$. Numbers indicate the time in μs elapsed from the start of a pulse (the pulse length is 42 μs).

Calibration of the used monochromator to an accuracy of 0.01 nm (Fig. 1, *a*) allowed us to identify features of the behavior of CsI lines of the $6p$–nd ($n = 7$–10) diffuse series. Experimentally determined shifts of these lines $\Delta\lambda_{exp}$ differ from calculated shifts $\Delta\lambda_{cal}$ (according to the data from [14]) at plasma parameters $n_e = 2 \cdot 10^{16}$ cm^{-3} and $T = 6000$ K, which may be regarded as reliably established within the spread of the experimental points in Fig. 6. With an increase in n, the difference between experimental and calculated shifts increases from 0.05 at $n = 7$ to 0.4–0.5 nm at $n = 10$ (see the table). For example, $\Delta\lambda_{exp} = 0$ for $n = 10$ ($\lambda = 563.521$ nm), and $\Delta\lambda_{cal} = -(0.4$–$0.6)$. This difference between $\Delta\lambda_{exp}$ and $\Delta\lambda_{cal}$ may be attributed to the influence of collisions of Cs atoms with Xe atoms (the Xe concentration is 30 times higher than the plasma concentration).

Figure 8 presents the temporal dependence of luminosity of certain CsI, XeI, KI, and RbI lines and the continuum emission at 500 nm. The temporal variation of the continuous background was taken into account in the case of CsI lines (672.2 and 723.2 nm). As for other lines, the background was insignificant and did not alter the nature of the temporal dependence of their luminosity. The luminosity

Calculated and experimental line shifts

λ, nm	Transition	Experimental shift, nm	Calculated shift, nm
563.521	$6p$–$10d$	0	−(0.4−0.6)
546.594	$6p$–$10d$	0	−0.2
566.401	$6p$–$9d$	−0.07	−0.2
601.04905	$6p$–$8d$	−0.05	−0.1
621.30998	$6p$–$8d$	−0.05	−0.1
672.329	$6p$–$7d$	−0.04	−0.04
697.330	$6p$–$7d$	−0.04	−0.1

of all CsI, RbI, KI, and NaI lines (including those that are not shown in Fig. 8) has a maximum at 30−31 μs (10−12 μs before the end of a pulse); this moment coincides with a knee in the n_e plasma concentration curve and the virtual attainment of n_e saturation, although temperature T continues to rise (Fig. 5). Certain lines (e.g., CsI 672.3 and KI 766.4; see Fig. 8) also have a well-defined maximum in decay, while the corresponding maxima of other lines are blurred. In contrast, all the recorded XeI lines intensify with a certain delay and reach their maximum luminosity immediately after the end of a pulse. This behavior of luminosity of most lines (the presence of two maxima) is attributed to the following fact. When plasma reaches a state close to complete ionization (for components with low ionization potential: Cs, Rb, K), the concentrations of atoms of these components in the ground state decrease sharply. This leads to a reduction in population of the excited levels of these components even with a continued growth of temperature T, which translates into a luminosity reduction and the formation of a maximum. In decay, the processes are reversed as one moves away from the state of complete ionization: the temperature drops (although not as rapidly), and the concentration of atoms in the ground state increases sharply.

In accordance with the above, we estimated the population of the upper level of the CsI 672.3 nm line ($7d$; $j = 3/2$; excitation potential, 3.23 eV). Ionization was considered to be equilibrium, and excited levels were assumed to be Boltzmann-populated. The calculation was performed for temperature dependence $T(t)$ determined experimentally (Fig. 5) and the value of $n_{a0} = 2 \cdot 10^{16}$ cm^{-3}, which is equal to plasma concentration n_e at the end of a pulse at the saturation stage (complete ionization). The luminosity of the CsI 672.3 line (normalized) is compared with the calculated equilibrium population in Fig. 9. The calculation yielded two maxima in the level population. It can be seen from the figure that the positions of these maxima and the dip between them and the leading edge of the population rise agree closely with similar features of the CsI 672.3 nm line luminosity curve. This provides yet another verification of thermal equilibrium in the discharge under

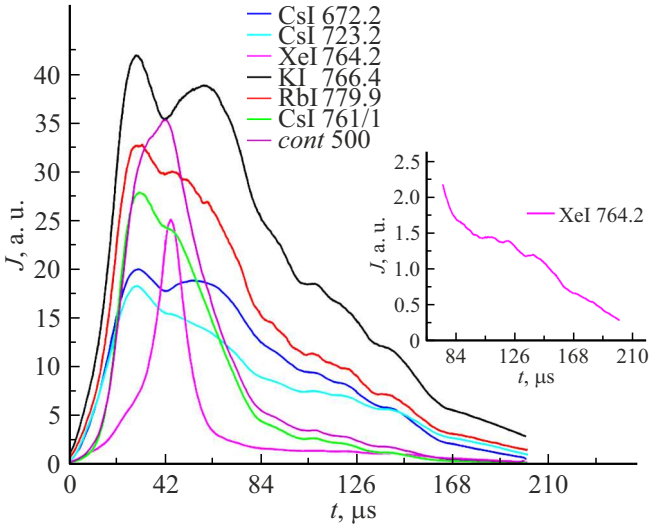

Figure 8. Dependence of the luminosity of lines and continuum on time for regime 2. XeI 764.2 nm line emission is shown on an enlarged scale in the inset.

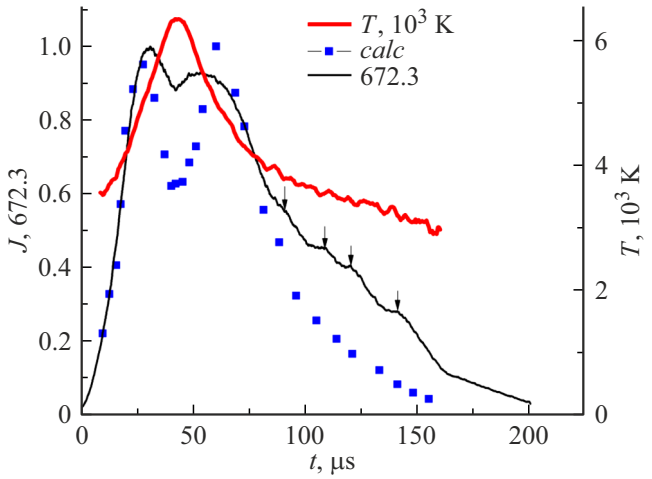

Figure 9. Comparison of luminosity of the CsI 672.3 line with the calculated equilibrium population of upper level $7d$, $j = 3/2$. Arrows indicate the luminosity maxima in decay.

consideration. The calculated dip between the maxima is noticeably deeper than the experimental one. This may be attributed to the radial dependence of T and n_{a0}, as a result of which the maximum population of the excited level at different points along the radius is reached at different moments in time. When the line luminosity is recorded, radiation from all points of the discharge located along the burner diameter is summed, which leads to smoothing.

In contrast to cesium, Xe is ionized very weakly in the studied regimes. For example, the equilibrium concentration of Xe^+ ions in regime 2 at the maximum temperature in a pulse of 6300 K is no greater than 10^{15} cm^{-3}, while the actual Xe^+ concentration is even less significant and is almost three orders of magnitude lower than the average concentration of Xe atoms. Therefore, the concentrations

of Xe atoms in the ground state do not depend on temperature, and the population of excited levels of Xe atoms follows temperature $T(t)$. Thus, as was already mentioned above, the maximum luminosity of xenon lines is reached immediately after the end of a current pulse (see, e.g., Fig. 8, XeI 764.2 line). The delay at the start of a pulse in the XeI line luminosity curve is attributable to a strong dependence of the population of excited levels on $T(t)$ ($\sim \exp(-E_k/kT)$, where E_k is the excitation energy of level k). Note that the initial section of the XeI 764.2 line luminosity in Fig. 8 is distorted under the influence of a weak background. After the end of a pulse, the luminosity of Xe lines decreases rapidly alongside with temperature, but the rate of luminosity decline slows down radically within 20 μs (Fig. 8 and the inset). This decay slowdown is attributable to the additional population of excited levels of XeI as a result of dissociative recombination of molecular Xe_2^+ ions, which, in turn, are formed as a result of conversion of atomic Xe^+ ions into molecular Xe_2^+. The constants of these processes are given in [16,17]. The conversion constant for Xe at room temperature is $k = 2 \cdot 10^{-31}$ cm^6/s, and the dissociative recombination coefficient is $\beta = 1.4 \cdot 10^{-6}$ cm^3/s. The values for a gas temperature in decay on the order of 3000 K should be reduced by a factor of 5–10. The estimated conversion and recombination times for the discharge parameters under consideration are close to 100 μs (conversion) and 10^{-4}–10^{-3} μs (dissociative recombination). Therefore, the overall duration of the recombination process is determined by conversion and is on the order of 100 μs. This value is consistent with the experimental decay time of the xenon line luminosity (see the inset in Fig. 8).

The plots of luminosity of lines of all elements present in the discharge (Cs, Xe, K, Rb) and the recombination continuum feature oscillations in decay (Figs. 8 and 9). These oscillations are especially pronounced in regime 1 (Fig. 10). In the present study, integral emission of the discharge from a region extended along the diameter of the burner was recorded. Naturally, this experimental procedure applies strong smoothing to local luminosity oscillations; i.e., the actual amplitude of local luminosity oscillations is significantly greater than the observed one. The maxima in all plots coincide in time, which is indicative of a common mechanism for the formation of these oscillations. Similar oscillations in decaying plasma of a pulsed discharge have been reported numerous times (see, e.g., [18,19]), typically in cylindrical tubes observed from their end. This measurement geometry provided an opportunity to record reliably the fluctuations in glow intensity of the axial region of a discharge and the variation of gas density in this region via interferometry. Macroscopic gas motion in a cesium lamp with a pulse-periodic discharge was calculated in [20,21]. The relatively slow heating of plasma during a pulse results in equalization of the total plasma pressure along the radius at any point in time within a pulse. The rate of radial displacement of gas is significantly lower than speed of sound v_s both during a pulse and after its end in decaying plasma on time scales much longer than the

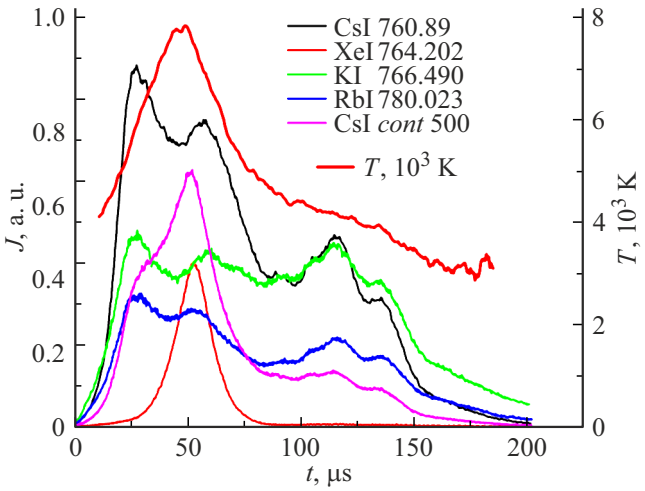

Figure 10. Temporal dependence of the luminosity of lines and continuum for regime 1.

pulse duration [20]. Our experimental data demonstrate that this conclusion is valid only within a pulse with a smooth (linear) increase in current from 0 to a maximum value of 50–100 A. In decay, oscillations of luminosity of the lines and the continuum arise after the sharp interruption of current and the cessation of energy input into plasma.

At the time the current is interrupted, gas is distributed very unevenly in the burner; the ratio of concentrations of the heavy component at the wall and on the axis is 4–5, which corresponds to the temperature ratio. A sufficiently rapid T reduction after the interruption leads to the emergence of a macroscopic gas motion toward the burner axis and subsequent density waves. One may estimate the period of such oscillations as $\tau = 2r/v_{s\mathrm{Xe}}$, where $v_{s\mathrm{Xe}}$ is the speed of sound in Xe. The speed of sound in gas is $v_s = (\gamma kT/M)^{1/2}$, where $\gamma = c_p/c_v$ is the ratio of heat capacities and M is the atom mass. At $T = 4000$ K in xenon, $v_{s\mathrm{Xe}} = 6.44 \cdot 10^4$ cm/s and $\tau = 8$ μs. The average distance between maxima is 16 μs and 13 μs in regimes 2 and 1, respectively. It is evident that the calculated and experimental values of oscillation period τ agree with each other.

It can be seen from Figs. 8 and 10 that the luminosity of lines drops almost to the noise level by 200 μs. Since the measurement of luminosity of lines at long times by means of increasing the width of monochromator slits is made virtually impossible by the rapid degradation of the photomultiplier tube [4], it is not yet possible to draw a conclusion about the characteristic decay time of these oscillations.

Conclusion

Detailed emission spectra of a cesium lamp with a pulse-periodic discharge were recorded at relatively low pressures and analyzed. These measurements included the examination of evolution of the recombination continuum

and the shape of spectral lines with time, which allowed us to determine the plasma parameters (temperature and electron concentration and their dependence on time) reliably. The plasma parameters determined by different methods are in reasonable agreement. The obtained data were interpreted within a simple model, and the existence of a local thermal equilibrium in plasma of this discharge was inferred. The examination of the shape variation of spectral lines over time provided an opportunity to identify qualitatively the processes of plasma generation and decay (by the broadening and shift of lines) and to establish the fact of displacement of atoms to the wall of the burner (by the emergence and growth of the dip in lines caused by absorption in the near-wall layer). Oscillations of luminosity of the continuum and lines in decay provide an indirect indication of the emergence of a macroscopic gas motion from the wall of the burner to its axis and subsequent density waves propagating in the radial direction.

Acknowledgments

The authors wish to thank A.M. Martsinovsky for helpful discussions and S.V. Gavrish for providing the single-ended cesium lamp.

Conflict of interest

The authors declare that they have no conflict of interest.

References

[1] S.V. Gavrish, V.B. Kaplan, A.M. Martsinovsky, I.I. Stolyarov. Prikl. Fiz., No. 5, 78 (2019) (in Russian).
[2] A.A. Bogdanov, S.V. Gavrish, A.M. Martsinovsky, I.I. Stolyarov. Usp. Prikl. Fiz., **8** (5), 326 (2020) (in Russian).
[3] F.G. Baksht, V.B. Kaplan, V.F. Lapshin, A.M. Martsinovskii. Tech. Phys. Let., **35** (12), 1078 (2009). DOI: 10.1134/S1063785009120037
[4] A.A. Bogdanov, A.M. Martsinovsky, I.I. Stolyarov. Tech. Phys., **69** (10), 1541 (2024). DOI: 10.61011/TP.2024.10.59358.105-24
[5] L. Agnew, C. Summers. *Proceedings of the VII International Conference on Phenomena in Ionized Gases* (Belgrade 1965), v. II, p. 574–580.
[6] L. Agnew, W.H. Reichelt. J. Appl. Phys., **39** (7), 3149 (1968). DOI: 10.1063/1.1656749
[7] A.A. Bogdanov, I.I. Stolyarov. Tech. Phys. Let., **49** (12), 101 (2023). DOI: 10.61011/TPL.2023.12.57599.100A
[8] N.B. Vargaftik, *Spravochnik po teplofizicheskim svoistvam gazov i zhidkostei* (Nauka, M., 1972) (in Russian).
[9] T.P. Red'ko. *Diffuziya normal'nykh i vozbuzhdennykh atomov metallov v gazakh.* In *Spravochnik konstant elementarnykh protsessov s uchastiem atomov, ionov, elektronov, fotonov*, Ed. by A.G. Zhiglinskii (Izd. S.-Peterb. Univ., SPb, 1994), pp. 206–224 (in Russian).
[10] W.A. Hamel, J.E.M. Haverkort, H.G.C. Werij, J.P. Woerdman. J. Phys. B: At. Mol. Phys., **19**, 4127 (1986). DOI: 10.1088/0022-3700/19/24/014
[11] *Termoemissionnye preobrazovateli i nizkotemperaturnaya plazma*, Ed. by B.Ya. Moizhes, G.E. Pikus (Nauka, M., 1973), p. 150 (in Russian).
[12] V.E. Cherkovets, N.G. Shestakova. Sov. Phys. Tech. Phys., **23** (2), 160 (1978).
[13] L.M. Biberman, V.S. Vorob'ev, I.T. Yakubov. *Kinetika neravnovesnoi nizkotemperaturnoi plazmy* (Nauka, M., 1982), p. 167 (in Russian).
[14] H.R. Griem. *Spectral line broadening by plasmas* (Academic Press, NY.–London, 1974)
[15] N. Konjević, M.S. Dimitrijević. W.L. Wiese. J. Phys. Chern. Ref. Data, **13** (3), 619 (1984). DOI: 10.1063/1.555715
[16] F.G. Baksht, V.G. Ivanov. Sov. Phys. Tech. Phys., **25** (3), 285 (1980).
[17] Yu.P. Raizer. *Fizika gazovogo razryada* (Intellekt, Dolgoprudny, 2009) (in Russian).
[18] Yu.G. Kozlov, A.M. Shuktin. Sov. Phys. Tech. Phys., **13** (9), 1197 (1969).
[19] T.V. Musienko, V.N. Skrebov. Sov. Phys. Tech. Phys., **28** (7), 786 (1983).
[20] F.G. Baksht, V.F. Lapshin. J. Phys. D: Appl. Phys., **41**, 205201 (2008). DOI: 10.1088/0022-3727/41/20/205201
[21] F.G. Baksht, V.F. Lapshin. Tech. Phys. Lett., **41** (1), 90 (2015). DOI: 10.1134/S1063785015010204

Translated by D.Safin